An Inter-strand Loop Extrusion Model

Andrea Bonato[1] and Davide Michieletto[1,2]

[1] *University of Edinburgh, SUPA, School of Physics and Astronomy, Peter Guthrie Road, EH9 3FD, Edinburgh, UK*[*]

[2] *MRC Human Genetics Unit, Institute of Genetics and Cancer, University of Edinburgh, Edinburgh EH4 2XU, UK*

Loop extrusion convincingly describes how certain Structural Maintenance of Chromosome (SMC) proteins mediate the formation of large DNA loops. Yet, most of the existing computational models cannot reconcile the recent observations that, while performing cis-extrusion, condensins can traverse each other and bypass large roadblocks *in vitro*. In this work, we propose an inter-strand model for loop extrusion which not only reproduces the experimental features of loop extrusion by one SMC complex, but also predicts the formation of so-called "Z-loops" via the interaction of two or more SMCs extruding along the same DNA substrate. By performing Molecular Dynamics simulations of this model we discover that the experimentally observed asymmetry in the different types of Z-loops is a natural consequence of the DNA tethering *in vitro*. Intriguingly, our model predicts this bias to disappear in absence of tethering and a third type of Z-loop, which has not yet been identified in experiments, to appear. We conclude discussing the implications of inter-strand loop extrusion on entangled DNA.

INTRODUCTION

Cells exert an impressive control over genome folding to confine long chromosomes inside the small space of a nucleus. Structural maintenance of chromosome (SMC) proteins are now well known to fundamentally contribute to the large-scale folding of DNA *in vivo* [1]. Cohesin and condensin, ring-shaped SMC protein complexes, can bring together two DNA segments and form DNA loops [2–4]. Certain SMCs do not appear to actively translocate along DNA in vitro, e.g. yeast cohesin has been shown to diffuse on DNA [5, 6] and to form clusters by bridging DNA [7] (although there is indirect evidence for translocation of yeast cohesin in vivo [8–10]). On the other hand, yeast condensin [11], human cohesin [12, 13], human condensin [14] and both cohesin and condensins in Xenopus egg extracts [15], have been directly shown to processively extrude loops in vitro.

The formation and growth of long DNA loops is well described by the loop extrusion model [2, 16–19]. First, loop extrusion factors (LEFs) such as condensin [11] or cohesin [12, 13] bind DNA and stem a short loop by grabbing two contiguous DNA segments; then, they move along the DNA until they either unbind or stop (e.g., *in vivo*, when they encounter the binding site of the zinc-finger protein CCCTC binding factor [20–22]). Evidence and models for entropic diffusion [5, 23–25], or bridging [26] have also been reported.

Although loop extrusion convincingly describes the principles behind the formation and growth of DNA loops, the mechanical details of how SMC protein complexes extrude loops are still debated. Proposed loop extrusion models include the pumping [27, 28], scrunching [29], tethered inchworm [30] and safety-belt [31] mixed with power stroke [32]; all inspired by the shape and structure of the SMC complexes [28, 33].

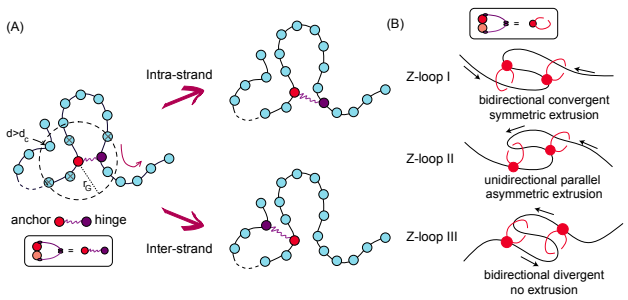

Figure 1. Illustration of the implemented extrusion rules. Periodically, the position along DNA of the LEF (spring connecting two beads of DNA) is updated according to a set of rules. Specific beads inside a sphere of radius r_G, the "grabbing" range, centred in the anchored end (red) of the LEF-spring (violet) are marked as selectable (see main text). One of these beads is chosen and the spring is replaced accordingly. Rarely, the selected bead will be far away (in DNA distance) from the base of the extruded loop (inter-strand grabbing). Beads marked with a cross are within grabbing range but, according to the rules, discarded from the selection. The thin red-purple arrow indicates the extrusion direction.

Most of the previously proposed models have a common feature, they assume the extrusion to happen in cis and by (quasi)topological entrapment of DNA within the SMC ring-like structure. An exception to these is the diffusion-capture model [34] which posits that DNA-bound SMCs can dimerize and form stable loops when they meet in trans by 3D diffusion. While both classes of models compare favorably well with experiments in vivo [35, 36], they both fall short to explain some recent observations in vitro. For instance, cis loop extrusion with topological entrapment cannot explain the for-

mation of so-called "Z-loops" [37], i.e. non-trivial positioning of SMCs yielding crossing looping topologies (see Fig. 1B), or the bypassing of roadblocks several times the size of condensin [38]. At the same time, loop-capture mechanisms [34, 36] cannot explain the observed processive extrusion of condensin on tethered DNA [11].

Motivated by this, and by SMC cohesin's key role to bridge sister chromatids *in vivo* (which cannot be achieved via a pure cis-looping mechanism) [39–41], here we propose an inter-strand model for loop extrusion. By performing Molecular Dynamics simulations, we discover that Z-loops are a natural consequence of introducing occasional inter-strand capture in a standard loop extrusion model (see Fig. 1). Furthermore, we find that the experimentally observed bias for Z-loop I over II may be a consequence of DNA tethering in the *in vitro* assay. Finally, we find that under certain conditions, i.e. when SMCs are initiated in series and in a convergent orientation, a third type of (non-growing) Z-loop appears. If confirmed by experiments, our model will carry some important consequences on the physics of DNA folding under inter-strand loops extrusion *in vivo*.

MODEL AND METHODS

We perform Molecular Dynamics simulations of a segment of DNA modelled as bead-and-spring polymer made of beads of size $\sigma = 10nm \simeq 30$ base-pairs. Consecutive beads are connected by finite-extension-nonlinear-elastic (FENE) bonds, i.e.

$$U_{\rm FENE}(r) = \begin{cases} -0.5 k_F R_0^2 \ln\left(1-(r/R_0)^2\right) & r \le R_0 \\ \infty & r > R_0 \end{cases}, \tag{1}$$

where $k_F = 30 k_B T/\sigma^2$ and $R_0 = 1.5\sigma$. Beads interact with each other via pure excluded volume, via a Weeks-Chandler-Andersen (WCA) potential,

$$U_{\rm WCA}(r) = \begin{cases} 4\epsilon\left[\left(\frac{\sigma}{r}\right)^{12} - \left(\frac{\sigma}{r}\right)^{6} + \frac{1}{4}\right] & r \le r_c \\ 0 & r > r_c \end{cases}, \tag{2}$$

where r denotes the separation between the bead centers and $r_c = 2^{1/6}\sigma$. The stiffness of DNA is accounted for by introducing a Kratky-Porod potential acting on triplets of consecutive beads along the polymer,

$$U_{\rm B}(i, i+1, i+2) = \frac{k_B T l_p}{\sigma}\left[1 - \frac{\mathbf{d}_{i,i+1}\cdot\mathbf{d}_{i+1,i+2}}{d_{i,i+1} d_{i+1,i+2}}\right], \tag{3}$$

where $\mathbf{r}_i$ is the position of i-th bead, $\mathbf{d}_{i,j} = \mathbf{r}_i - \mathbf{r}_j$ and $d_{i,j} = |\mathbf{r}_i - \mathbf{r}_j|$ are, respectively, the separation vector between beads i and j and its modulus. We set $l_p = 5\sigma$ to achieve the known persistence length of DNA $l_p \simeq 50$ nm [42]. We use LAMMPS [43] engine to integrate the equations of motion with implicit solvent (Langevin dynamics) with friction $\gamma = m/\tau_B$ (where the Brownian time is $\tau_B = \gamma\sigma^2/k_B T$) is related to the thermal noise amplitude via the fluctuation-dissipation theorem. Finally, the integration step size is $10^{-4}\tau_B$.

The inter-strand loop extrusion model

In this section we explain in detail our inter-strand loop extrusion model. In essence, we aim to generalise the standard cis loop extrusion model [16, 17] by introducing the possibility of trans (3D) moves in which LEFs can grab a DNA segment that is proximal in 3D. Each SMC is modelled as a spring connecting two DNA beads (segments), and is described by the harmonic potential

$$U_H = k\left(r - r_0\right)^2, \tag{4}$$

where r_0 is the resting distance between the centers of the two beads and k is the elastic constant (see below for their values). To reproduce the unidirectionality of loop extrusion by condensin [11], one of the two ends of the spring is anchored to one specific bead (the loading site) for the duration of the simulation, whereas the other is periodically moved from bead to bead following a given set of rules that we shall discuss below. To account for the size of SMC complexes (e.g. about 40 nm for cohesin [44] and 50 nm for condensin [45]), we increase the excluded volume of the two beads connected by the spring; this is done by using phantom beads so that the DNA substrate is not deformed (see Figs. 2A and 3H,I).

The rules for the inter-strand loop extrusion are the following: First, after a LEF is loaded with its anchor at bead l and hinge at bead m, we randomly choose an extrusion direction. Then, at each extrusion step, all the beads within a certain "grabbing" Euclidean distance r_G from the anchor l are identified (see Fig. 1). Importantly, we set r_G to be smaller than the known size of SMCs, i.e. about 50 nm (see Table I). Out of those 3D proximal beads, we select two groups: the first contains all the intrachain beads that are within d_C beads from the hinge m and, according to the extrusion direction, either to its left or to its right (beads $k \ge m$ or $k \le m$). The parameter d_C thus works as a threshold on 1D proximity as the LEF can in principle grab up to the $d_C = 5$ nearest neighbour in 1D. The second group contains the beads farther than d_C in 1D from both the hinge m and the anchor l. The reason for introducing these groups is purely technical: we want to algorithmically distinguish beads that are close in 3D but far in 1D and at the same time disallow back-steps which are only rarely seen in experiments. The lack of back-steps is also a standard assumption in cis loop extrusion [17]. After the creation of these two groups, we randomly select one bead, n, from either the first (1D) group or, if not empty, from the second (3D) group, with a small probability p_{inter}. To update the position of the LEF, we delete the spring connecting l to m

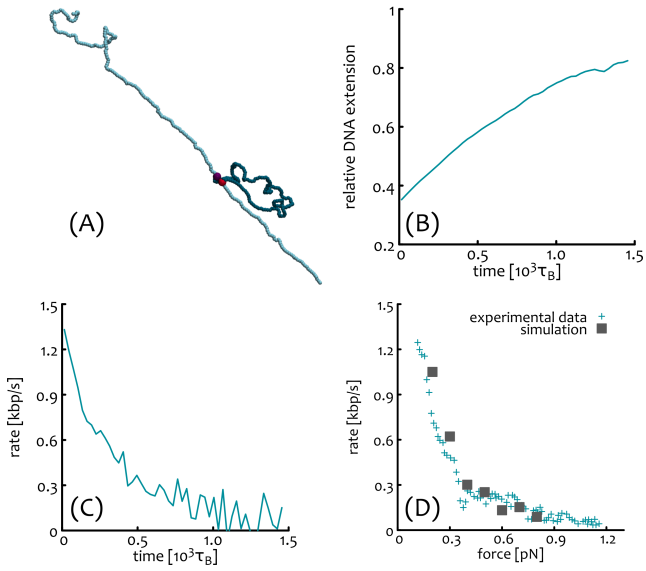

Figure 2. **(A)** MD simulations of doubly tethered DNA (cyan) loaded with one asymmetric LEF (violet and red) extruding a loop (blue). **(B)** Mean relative DNA extension as a function of time. The relative extension is defined as the end-to-end distance divided by the difference between the total length of the DNA and the length of the extruded loop. **(C)** Extrusion rate as a function of time. **(D)** Extrusion rate as a function of tension: comparison between our simulations (dark grey squares) and experimental data from Ref. [11] (cyan +).

and add a spring connecting l to n. The process of moving the spring is identified as an intra-strand jump if n is in the first (1D) group, inter-strand jump (or "grabbing") otherwise. In the second case, a new extrusion direction is selected randomly as we assume that the SMC cannot distinguish forward/backward on a newly grabbed DNA segment. Finally, we note that setting $p_{inter} = 0$ and $d_C = 2$ maps our model back to standard cis-only loop extrusion models.

As mentioned above, we implement this algorithm in LAMMPS [43]. In practice we do this by loading LAMMPS as an external library within a C++ program. Every 8000 LAMMPS steps (or $0.8\tau_B$), we extract the coordinates of all the beads and loop over the positions of LEFs. For each one of the LEFs, we update their position following the rules described above and with a probability $p \ll 1$. The bonds are then updated using the "create bond" and "delete bond" commands. Sample codes can found at `https://git.ecdf.ed.ac.uk/dmichiel/translefs`.

Parameter	Symbol	value
Size of bead	σ	$10nm$
grabbing range 3D	r_G	3.4σ
LEF update time	dt	$0.8\tau_B$
LEF spring stiffness	k	$4k_BT/\sigma^2$
LEF rest length	r_0	1.6σ
inter-strand catch probability	p_{inter}	5×10^{-3}
size of LEF	σ_c	3.2σ
Brownian time	τ_B	$0.011s$
1D cis step	d_C	5σ

Table I. Table of key parameters of the model. The combination of values of Brownian time τ_B, LEF update time dt and LEF spring stiffness k and rest distance r_0 were chosen to match the extrusion rate experimentally measured in Ref. [11]. The interstrand probability p_{inter} is only relevant when two LEFs are extruding along the same substrate and it regulates how often a LEF catches a 3D proximal DNA segment.

RESULTS

Calibration of the model using one LEF

We first perform simulations of doubly tethered DNA $N = 400$ beads long loaded with one (asymmetric) LEF (Fig. 2A) in order to calibrate the parameters of our model against experimental observables, such as extrusion rate (Ref. [11]).

Each initial conformation is obtained by equilibrating for a long time ($10^6\tau_B$, see Methods) a polymer with the constraint that the Euclidean distance between its two ends is equal to one third of its total length when pulled taut. This choice is to mimic the experimental set up in Ref. [11] and is practically implemented by applying a force to the chain ends until they reach a distance of $N/3$ in a pre-simulation step and then by equilibrating the chain with its ends fixed in space. After equilibration, a LEF is loaded either at bead $N/6$ and with positive extrusion direction (i.e. the moving side of the spring with progressively larger bead index) or at bead $5N/6$ and with negative extrusion direction. In this way, we prevent the extrusion process to end because of the LEF reaching the end of the polymer.

Importantly, in our simulations, the extrusion rate is not a fixed parameter, but depends on the tension experienced by the polymer during the loop extrusion as this enters in competition with the tethered ends. For instance, in Fig. 2B, one can appreciate that the relative DNA extension, i.e. the ratio between the end-to-end distance (R_{ee}) and the difference of DNA length (N) and extruded loop length ($l = l(t)$), or $R_{ee}/(N - l)$, grows in time because the difference $N - l$ becomes smaller and R_{ee} is kept constant. At large times, when the loop extrusion step is balanced by the tension on the DNA, one

expects to see a plateau in the relative extension. This stalling is due to the fact that in the LEF update rule, new segments are searched within a radius r_G from the LEF anchor point. If the LEF bond connecting anchor and hinge is $\simeq r_G$ (notice that $r_G \simeq 2r_0 \simeq 32$ nm), segments outside the extruded loop do not fall within the grabbing range of the LEFs. In other words, the tension along the polymer leads to stretching of the LEF bond and then to stalling via the depletion of available cis (and trans) segments that can be grabbed.

The extrusion rate is thus computed from the simulations by taking the time derivative of the length of the extruded loop as in experiments (Fig. 2C), i.e. $rate = \partial l(t)/\partial t$. We then plot the rate as a function of the tension by converting the extension of the polymer to force as done in Ref. [11], i.e. by using a tabulated conversion (see github repository). Fig. 2D shows the rate-force curve obtained by simulating 100 DNA molecules.

The free parameters of the model are (i) LEF update time dt, i.e. the time in between two LEF moves, (ii) LEF spring stiffness k, (iii) rest length r_0 and (iv) Brownian time τ_B. They were progressively tuned to closely match the experimental data in Ref. [11] and are reported in Table I. With this calibration we thus lock in a combination of these parameters that match experimental data on single LEF extrusion on tethered DNA and leave the inter-strand grabbing parameter p_{inter} free to be explored when studying multiple LEFs.

Modelling interactions of two LEFs

After having calibrated our model using one LEF to match the experimentally observed behaviour, we now perform MD simulations of two LEFs along the same DNA substrate (see Fig. 3H,I). To capture the experimental setup of Ref. [37], we simulate doubly tethered polymers $N = 400$ beads long and choose to load the LEFs in a nested state, as typically observed in experiments. This is done by (i) loading the first LEF immediately after equilibration in a random position and with random extrusion direction and then (ii) by attempting loading the second LEF inside the loop formed by the first some time after the simulation starts. We can distinguish between two further cases: in one half of the simulations, the two LEFs are nested and extruding in the same direction (Fig. 3F) while in the second half the LEFs have opposite extrusion direction (Fig. 3G).

To check the evolution of the polymer topology over time, we reconstruct the position of the ends of the LEFs and draw a corresponding arch diagram for each observed configuration (Fig. 3A-E). Briefly, we observe separated, nested and 3 types of Z-loop structures. It should be noted that all these structures are non-equilibrium topologies since the LEFs are unidirectionally moving along the DNA. This means that at very large times we expect LEFs to reach an absorbing state from which they cannot recover. This is also the case in experiments, if ran long enough and in the case of no SMC unloading. Our simulations total runtime is shorter than the time it takes for the LEFs to reach an absorbing state. Additionally, the same structure can appear more than once for each simulation: it can form, undo and eventually form again at a later time. A step-wise scheme of loop formation and disassembly is reported in SI, Fig. S5. We stress that it is not the loops themselves that are undone, but the Zloop structures formed by the interaction of the two loops.

To best compare with experiments, we align to the method of Ref. [37] and record (i) the number of times we observe a given loop(s) topology and (ii) its survival time from the start of the simulation and for a fixed total simulation runtime. Fixing a total runtime is important as the final states are absorbing and would therefore dominate the spectrum of topologies in the large time limit.

In Fig. 3J,K we show the relative frequency and survival times of the 5 different topologies. As one can notice, while the nested state is the most likely topology, Z-loops I and II are also significant. Remarkably, we observe a spontaneous asymmetry in topologies, whereby Z-loop I (Z_I) is more than twice as likely to form than Z-loop II (Z_{II}), i.e. $Z_I/Z_{II} \simeq 2.5$. This asymmetry emerges naturally, without imposing any bias favouring the formation of a particular Z-loop type. Additionally, it is in good agreement with experiments, as they report $Z_I/Z_{II} \simeq 3$ [37]. We find that this asymmetry is assay and tension dependent, and that singly-tethered DNA display a far weaker bias in Z_I/Z_{II} (see next section).

We finally highlight that while we observe Z-loop III (Z_{III}) in simulations (Fig. 3E), they have not been detected in experiments [37]. Accordingly, the frequency with which they appear in our simulations is tens of times smaller than the other Z-loop topologies. Again, we predict that this result is assay-dependent (see below).

Z-loop asymmetry is due to tension

We can think of at least two reasons that may bias the formation of Z_I over Z_{II}. As sketched in Fig. 4, because of the doubly-tethered assay, more frequent inter-grabbing events are expected to occur on the side of the anchor of the outermost LEF (labelled b in Fig. 4A,B). This is because the extrusion is unidirectional and the DNA, being tethered, has a preferred structural direction in the 3D space (the line passing through the two fixed ends). Each time a loop extruded by the external LEF grows, a new segment of DNA is brought inside the loop. Since the DNA is tethered, and especially when the relative DNA extension is close to one, the angle between this newly added segment and the geometric line passing through the two ends of the DNA is small (see Fig. 4A).

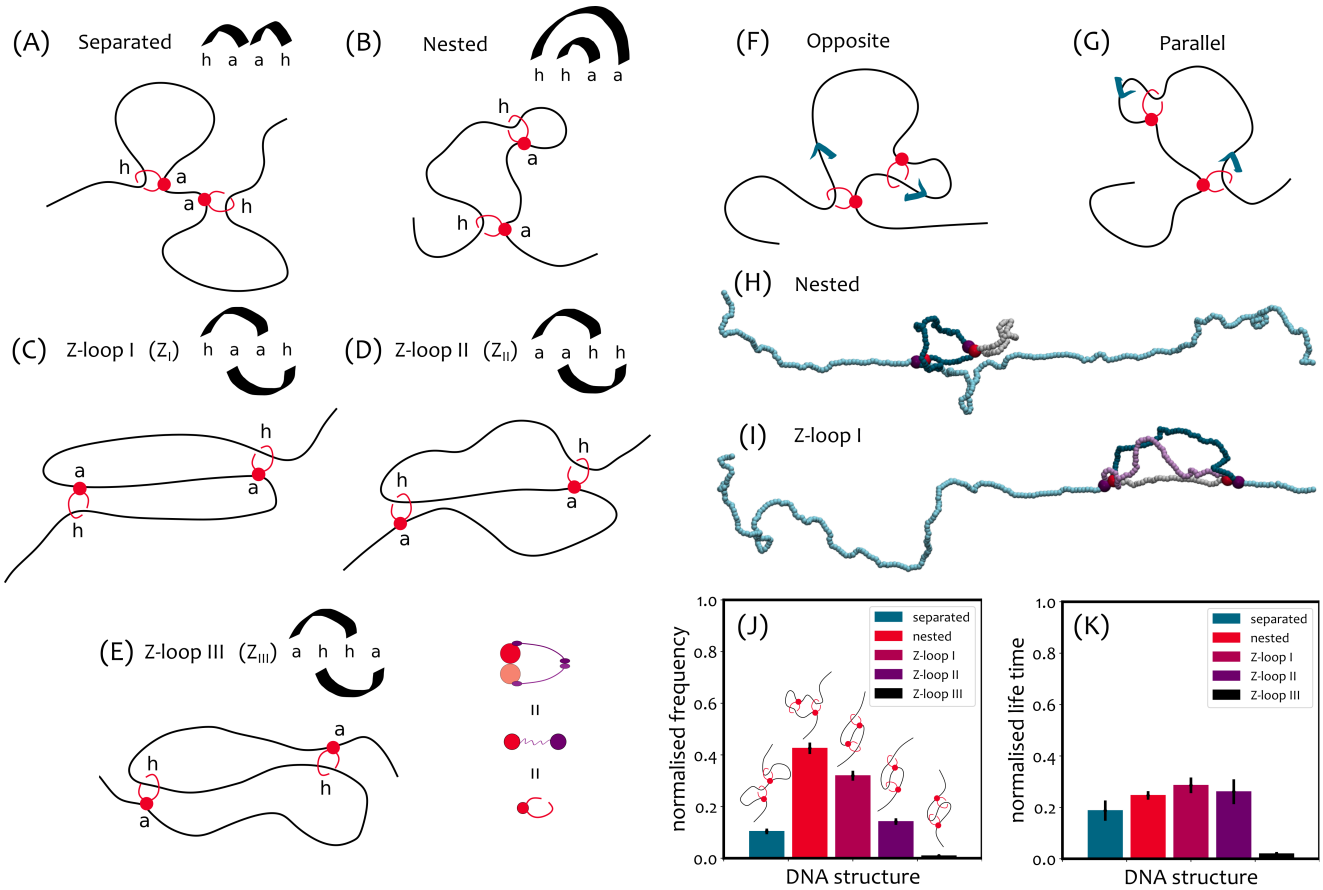

Figure 3. **(A)-(E)** A summary of the 5 potential Z-loop structures observed in simulations with two LEFs (the anchored bead "a" and the moving hinge "h"): **(A)** separated, **(B)** nested, **(C)** Z-loop I (this structure grows or shrinks as DNA reels in or out from the boundaries of the loop depending on the LEFs orientation); **(D)** Z-loop II (only one of the boundaries moves with respect to the structure); **(E)** Z-loop III (both boundaries of the structure are fixed as the anchors are external to the moving hinges. See also SI Fig. S5 for a step-wise scheme on the formation of these loop topologies. **(F)(G)** Schematic illustration of the initial configuration of MD simulations with two nested LEFs. When the second LEF is loaded, its extrusion direction either opposes **(F)** or copies **(G)** the extrusion direction of the first one. Blue arrows indicate in which direction DNA is reeled inside a loop. **(H)(I)** MD simulations of doubly tethered DNA loaded with two LEFs. **(H)** When the LEFs are nested, one of the loops (grey) extruded by the two protein complexes is part of the other loop (grey+blue). **(I)** Two condensins can fold a Z-loop (type I in the figure). One of the three segments (grey) involved in a Z-loop is shared between the loops extruded by the two condensins (grey+blue and grey+lilac). **(J)(K)** Frequency **(J)** and survival times **(K)** of topological structures in simulations of two nested LEFs on doubly tethered DNA.

As shown in Fig. 4A (see also snapshots in Figs. 2A and 3H), as the extrusion goes on, the geometry of the extruding complexes biases the extruded DNA loop to fold over the anchor (where there is no force applied by the LEF). As a consequence, due to closer proximity, it then becomes easier for the nested LEF to grab a segment behind the anchor of the external LEF (side b) thereby folding a Z_I (Fig. 4B), rather than grabbing a segment over the hinge of the other LEF (side a) to eventually form a Z_{II}.

Moreover, when two nested LEFs are both extruding in the same direction along the DNA, one of them is "running away" from the other. As shown in Fig. 4C, this hinders the hinge of the nested LEF to jump over the other when folding a Z_{II}. This suggests that directionality of LEFs also play a role in which Z-loop topology are formed, as seen in simulations (see SM).

Singly- vs doubly-tethered DNA

As mentioned in the previous section, the tethering of the DNA may bias the local conformation of extruded loops especially in the limit where the relative extension is close to one. To test this hypothesis, we simulate two nested LEFs on singly-tethered DNA. While this setup was considered in experiments [37], the microscope resolution did not allow a clear interpretation of the looped topologies. On the contrary, here we can precisely classify and distinguish different topologies and Z-loops. As

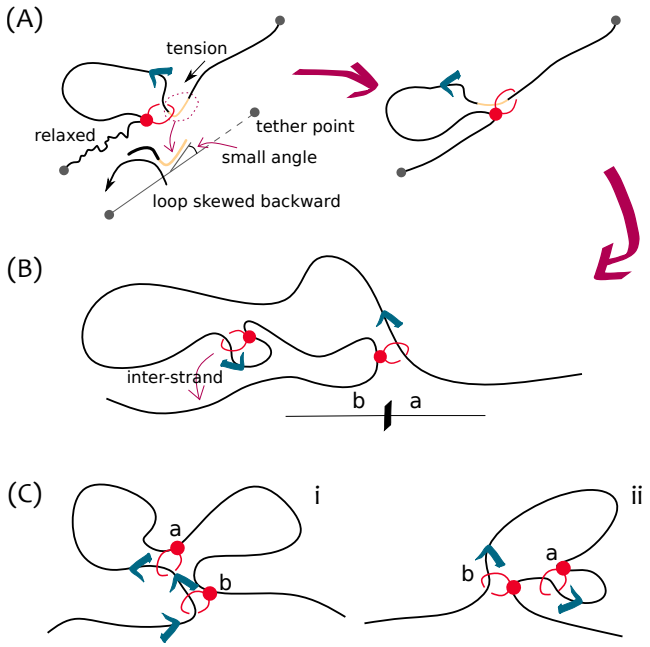

Figure 4. Addressing the asymmetry in the frequency of Z_I and Z_{II} on DNA with two tethered ends. **(A)** At each extrusion step, the segment of DNA (cream) on the intake side is likely to be pulled taut and roughly parallel to the line connecting the two ends of the tethered DNA. The anchor-side part is instead relaxed as no tension is applied. **(B)** This effective alignment biases the extruded loop to fold over the anchor-side of the most external LEF. In turn, this favours the nested LEF to grab segments of DNA from over the anchor side (b) rather than over the hinge side (a) (see Fig. 2A). **(C) (i)** If the two nested LEFs are extruding in the same direction and the internal LEF, labelled a, approaches the other one (b), a Z_{II} is formed when a's hinge jumps other b's. When the jump is attempted, however, b's hinge is running away from a's. **(C) (ii)** If instead the LEFs are extruding in opposite directions, a Z_I is formed when a's hinge jumps other b's anchor, which does not move. Move **(ii)** (yielding Z_I) is more likely to succeed due to the slower dynamics of the polymer near a LEF anchor.

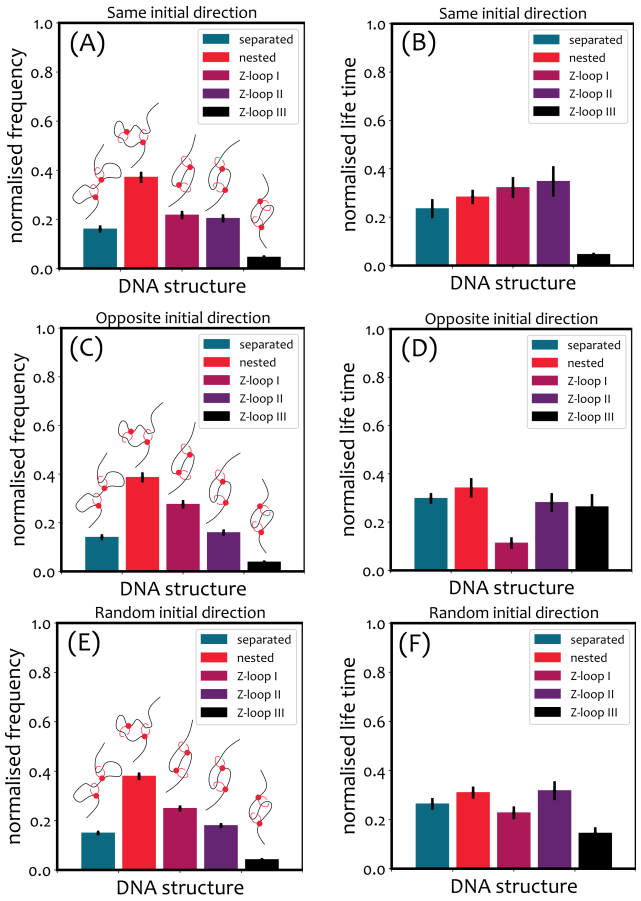

Figure 5. Results of simulations of nested LEFs on singly-tethered DNA. **(A)(C)(E)** Frequency of topologies folded by two LEFs loaded with the **(A)** same or **(C)** opposite initial directions. **(B)(D)(F)** Mean normalised life time of the loop topologies.

before, we can also distinguish between nested LEFs extruding in parallel versus opposite directions. As shown in Fig. 5, we observe that, compared with the doubly-tethered case, here the frequency of Z_I and Z_{II} are more similar to each other than in the doubly-tethered case. In other words no Z_I/Z_{II} bias is detected for singly-tethered DNA. We argue that this should also hold for free DNA. Finally, the fraction of Z_{III} is now larger than before, but still significantly lower than $Z_{I,II}$; yet, the corresponding mean (normalised) life time is substantially larger (see Fig. 5D), meaning that it forms relatively rarely, but when it does, it is a stable structure.

These results confirm that, as hypothesised in the previous section, tethering the ends of DNA favours the formation of Z_I; and we may thus conjecture that the statistics of Z-loop formation *in vivo* could differ from those observed *in vitro* [37]. To test our prediction, that DNA tension and assay affect the statistics of Z-loops, more *in vitro* experiments with a different choice of set ups are needed.

Z-loop formation depends on initial loading

Until now we have only considered situations in which the LEFs started from a nested configuration. This is frequently observed in experiments, as condensins favour binding to bent or supercoiled substrates [46–48]. On the other hand, in our simulations we can also study the case in which LEFs start in a serial (separated) state rather than nested.

To this end we load two LEFs at random on an equilibrated doubly-tethered polymer and impose them to have opposite extrusion directions. We simulate 50 polymers and collect the results in Fig. 6: the measured frequencies (Fig. 6A) and mean normalised life times (Fig. 6B)

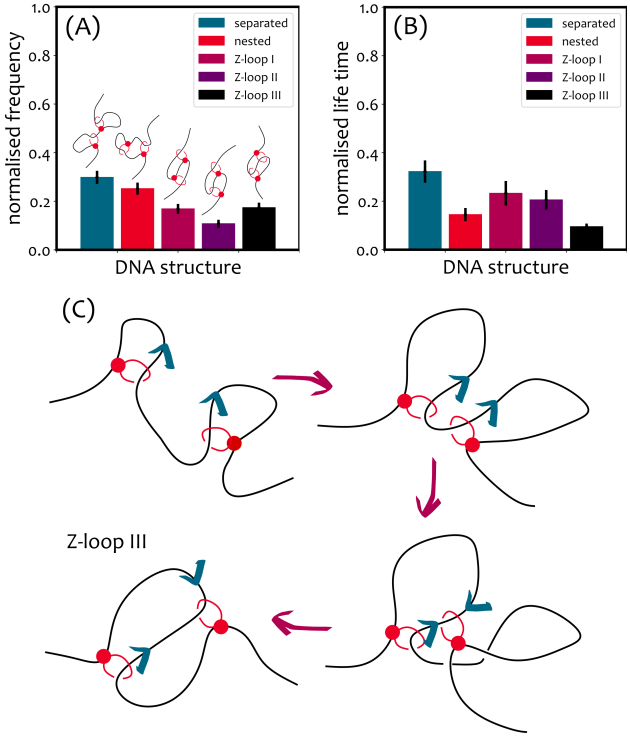

Figure 6. **(A)(B)** Results of simulations of two initially separated LEFs loaded on doubly-tethered DNA with opposite initial extrusion directions. Frequency **(A)** and mean normalised life time **(B)** of the structures. **(C)** Scheme of the formation of a Z_{III} in simulations with two initially separated LEFs and opposite extrusion directions. Z_{III} is formed if one of the hinges jumps over the other.

differ substantially from those estimated for two initially nested LEFs. Specifically, the frequency of Z_I remains larger than Z_{II}, however the fraction of Z_{III} is much more significant, as it rivals the fraction of Z_I. This is not surprising: the formation of Z_{III} is expected when the hinges of two LEFs meet and one jumps over the other (see Fig. 6C).

CONCLUSIONS

Motivated by the observation of the formation of Z-loops *in vitro*, we have proposed an inter-strand loop extrusion model for generic SMC on doubly- or singly-tethered DNA.

First, we have calibrated our model to match the experimental force-rate curve of a single condensin extruding loops on doubly-tethered λ-DNA [11]. Then, using the so-determined parameters, we have studied the types of topologies that can emerge when two LEFs are set to extrude loops on the same DNA substrate.

Importantly, we have identified 5 different loop topologies: separated (or serial), nested (or parallel) and 3 types of Z-loops. These are most clearly classified in terms of their net extrusion capability: Z_I can extrude from both boundaries, Z_{II} can extrude from only one of the two boundaries while Z_{III} cannot extrude loops as the anchors of the LEFs are facing outward. We highlight that the ratio of Z_I/Z_{II} observed in our simulations is in good agreement with the one in recent experiments [37] ($Z_I/Z_{II} \simeq 2.5 - 3$).

We conjectured that this asymmetry in formation of Z-loops was due to the details of the assay. In particular,we find that loop extrusion on doubly-tethered DNA induces geometric conformations that favour 3D proximity of the internal LEF with the segments of DNA on the outside of the most external LEF's anchor (Fig. 4B). This effectively biases the statistics towards Z_I where both hinges face outward of the Z-loop. To test this hypothesis, we studied the formation of Z-loops on singly-tethered DNA and indeed observed that Z_I are in this case as likely as Z_{II}. The singly-tethered DNA assay was also performed in Ref. [37] but due to the limits of optical resolution the authors could not classify the type of the Z-loops formed.

Finally, we find that Z_{III} folds frequently if the LEFs are initially separated and extruding in opposite directions as in this case it is likely that the hinges jump over each other and leave the static anchors on the outside of the Z-loop. This is a prediction of our simulations that could be tested in experiments by forcing the loading of condensins on two separated sites rather than nested.

We conclude highlighting that the precise mechanics of DNA loop extrusion is still highly debated. Here we have not attempted to give a precise biochemical characterisation of the steps involved with extrusion (for this see e.g. Ref. [49]). Instead, we have focused on relaxing the assumption of cis extrusion, which may be difficult to justify in (i) entangled conditions and (ii) non-topological models of loop extrusion, i.e. where condensin/cohesin do not topologically embrace the DNA substrate [50, 51]. Intriguingly, recent in vitro evidence provided direct evidence that loop extrusion is non-topological [38] and that some SMCs can form long-range bridges [7]. In light of this, inter-strand grabbing cannot be excluded based on structural or topological considerations and may be particularly likely to occur in dense DNA conditions.

We argue that two types of experiments may help to disentangle this problem. First, single molecule set ups using two entangled DNA molecules in an "X" configuration as in Ref. [6]; these could give a clear evidence of SMCs jumping/bridging and at the same time extruding. Second, we argue that experiments performed on bulk solutions of entangled DNA with and without SMCs may display different viscoelastic properties depending on whether SMCs can extrude only in cis or also in trans.

We hope our findings help to understand and rationalise the appearance of Z-loops *in vitro*. Additionally, and perhaps most importantly, we feel that our work suggests that more comprehensive models of loop extrusion

may be needed to explain the organisation of DNA *in vivo*. Currently, many models for interphase and mitotic genome organisation employ cis loop extrusion [16, 17], yet it is well known that cohesin bridges sister chromatids together and without it the mitotic structure would fall apart [39–41]. We thus argue that some SMCs, and in some conditions, may be able to activate a trans-loop extrusion mechanisms with profound consequences on the organisation and dynamics of genomes *in vivo*.

ACKNOWLEDGEMENTS

DM is a Royal Society University Research Fellow. This work was supported by the ERC (TAP, 947918). The code to simulate inter-strand loop extrusion was developed by AB and is deposited open access at `https://git.ecdf.ed.ac.uk/dmichiel/translefs`.

* a.bonato@sms.ed.ac.uk

[1] M. Hirano and T. Hirano, EMBO J. **21**, 5733 (2002).
[2] K. Nasmyth, Nat. Cell Biol. **13**, 1170 (2011).
[3] F. Uhlmann, Nat. Rev. Mol. Cell. Biol. **17**, 399 (2016).
[4] T. Hirano, Cell **164**, 847 (2016).
[5] J. Stigler, G. Ö. Çamdere, D. E. Koshland, and E. C. Greene, Cell Rep. **15**, 988 (2016).
[6] P. Gutierrez-Escribano, M. D. Newton, A. Llauró, J. Huber, L. Tanasie, J. Davy, I. Aly, R. Aramayo, A. Montoya, H. Kramer, J. Stigler, D. S. Rueda, and L. Aragon, Science Advances **5**, 1 (2019).
[7] J.-K. Ryu, C. Bouchoux, H. W. Liu, E. Kim, M. Minamino, R. de Groot, A. J. Katan, A. Bonato, D. Marenduzzo, D. Michieletto, F. Uhlmann, and C. Dekker, Science Advances **7**, eabe5905 (2021).
[8] E. F. Glynn, P. C. Megee, H. G. Yu, C. Mistrot, E. Unal, D. E. Koshland, J. L. DeRisi, and J. L. Gerton, PLoS Biology **2** (2004), 10.1371/journal.pbio.0020259.
[9] A. Lengronne, Y. Katou, S. Mori, S. Yokabayashi, G. P. Kelly, T. Ito, Y. Watanabe, K. Shirahige, and F. Uhlmann, Nature **430**, 573 (2004).
[10] F. Paldi, B. Alver, D. Robertson, S. A. Schalbetter, A. Kerr, D. A. Kelly, J. Baxter, M. J. Neale, and A. L. Marston, Nature **582**, 119 (2020).
[11] M. Ganji, I. A. Shaltiel, S. Bisht, E. Kim, A. Kalichava, C. H. Haering, and C. Dekker, Science (80-.). **360**, 102 (2018).
[12] I. F. Davidson, B. Bauer, D. Goetz, W. Tang, G. Wutz, and J.-M. Peters, Science **366**, 1338 (2019).
[13] Y. Kim, Z. Shi, H. Zhang, I. J. Finkelstein, and H. Yu, Science **366**, 1345 (2019).
[14] M. Kong, E. E. Cutts, D. Pan, F. Beuron, T. Kaliyappan, C. Xue, E. P. Morris, A. Musacchio, A. Vannini, and E. C. Greene, Molecular Cell **79**, 99 (2020).
[15] S. Golfier, T. Quail, H. Kimura, and J. Brugués, eLife **9**, 1 (2020).
[16] G. Fudenberg, M. Imakaev, C. Lu, A. Goloborodko, N. Abdennur, and L. A. Mirny, Cell Rep. **15**, 2038 (2016).
[17] A. Goloborodko, J. F. Marko, and L. A. Mirny, Biophys. J. **110**, 2162 (2016).
[18] A. L. Sanborn, S. S. P. Rao, S.-C. Huang, N. C. Durand, M. H. Huntley, A. I. Jewett, I. D. Bochkov, D. Chinnappan, A. Cutkosky, J. Li, K. P. Geeting, A. Gnirke, A. Melnikov, D. McKenna, E. K. Stamenova, E. S. Lander, and E. L. Aiden, Proc. Natl. Acad. Sci. USA **112**, 201518552 (2015).
[19] E. Alipour and J. F. Marko, Nucleic Acids Res. **40**, 11202 (2012).
[20] J. E. Phillips and V. G. Corces, Cell **137**, 1194 (2009).
[21] Z. Tang, O. J. Luo, X. Li, M. Zheng, J. J. Zhu, P. Szalaj, P. Trzaskoma, A. Magalska, J. Wlodarczyk, B. Ruszczycki, P. Michalski, E. Piecuch, P. Wang, D. Wang, S. Z. Tian, M. Penrad-Mobayed, L. M. Sachs, X. Ruan, C. L. Wei, E. T. Liu, G. M. Wilczynski, D. Plewczynski, G. Li, and Y. Ruan, Cell **163**, 1611 (2015).
[22] M. Oti, J. Falck, M. A. Huynen, and H. Zhou, BMC Genomics **17**, 252 (2016).
[23] C. Brackley, J. Johnson, D. Michieletto, A. Morozov, M. Nicodemi, P. Cook, and D. Marenduzzo, Phys. Rev. Lett. **119**, 138101 (2017).
[24] I. F. Davidson, D. Goetz, M. P. Zaczek, M. I. Molodtsov, P. J. Huis in 't Veld, F. Weissmann, G. Litos, D. A. Cisneros, M. Ocampo-Hafalla, R. Ladurner, F. Uhlmann, A. Vaziri, and J. Peters, EMBO J. **35**, 2671 (2016).
[25] T. Yamamoto and H. Schiessel, Phys. Rev. E **96**, 1 (2017).
[26] J.-K. Ryu, C. Bouchoux, H. W. Liu, E. Kim, M. Minamino, R. de Groot, A. J. Katan, A. Bonato, D. Marenduzzo, D. Michieletto, F. Uhlmann, and C. Dekker, Sci. Adv. **7**, 1 (2021).
[27] J. F. Marko, P. De Los Rios, A. Barducci, and S. Gruber, Nucleic Acids Research **47**, 6956 (2019).
[28] M. L. Diebold-Durand, H. Lee, L. B. Ruiz Avila, H. Noh, H. C. Shin, H. Im, F. P. Bock, F. Bürmann, A. Durand, A. Basfeld, and et al., Molecular Cell **67**, 334 (2017).
[29] T. Terakawa, S. Bisht, J. M. Eeftens, C. Dekker, C. H. Haering, and E. C. Greene, Science (80-.). **676**, eaan6516 (2017).
[30] M. H. Nichols and C. V. G, Nature Structural & Molecular Biology **25**, 906 (2018).
[31] M. Kschonsak, F. Merkel, S. Bisht, J. Metz, V. Rybin, M. Hassler, and C. H. Haering, Cell **171**, 588 (2017).
[32] S. K. Nomidis, E. Carlon, S. Gruber, and M. J. F, bioRxiv , 2021.03.15.435506 (2021).
[33] K. Kamada, M. Suétsugu, H. Takada, M. Miyata, and T. Hirano, Structure **25**, 603 (2017).
[34] T. M. Cheng, S. Heeger, R. A. Chaleil, N. Matthews, A. Stewart, J. Wright, C. Lim, P. A. Bates, and F. Uhlmann, eLife **4**, 1 (2015).
[35] J. H. Gibcus, K. Samejima, A. Goloborodko, I. Samejima, N. Naumova, J. Nuebler, M. T. Kanemaki, L. Xie, J. R. Paulson, W. C. Earnshaw, L. A. Mirny, and J. Dekker, Science (80-.). **359** (2018), 10.1126/science.aao6135.
[36] T. Gerguri, X. Fu, Y. Kakui, B. S. Khatri, C. Barrington, P. A. Bates, and F. Uhlmann, Nucleic acids research **49**, 1294 (2021).
[37] E. Kim, J. Kerssemakers, I. A. Shaltiel, C. H. Haering, and C. Dekker, Nature **579**, 438 (2020).
[38] B. Pradhan, R. Barth, E. Kim, I. F. Davidson, B. Bauer, T. van Laar, W. Yang, J.-K. Ryu, J. van der Torre, J.-M. Peters, and C. Dekker, bioRxiv (2021),

10.1101/2021.07.15.452501.
[39] K. Nasmyth and C. H. Haering, Annu. Rev. Genet. **43**, 525 (2009).
[40] Y. Murayama, C. P. Samora, Y. Kurokawa, H. Iwasaki, and F. Uhlmann, Cell **172**, 465 (2018).
[41] E. Piskadlo, A. Tavares, and R. A. Oliveira, Elife **6**, 1 (2017).
[42] C. Bustamante, J. F. Marko, E. Siggia, and S. B. Smith, Science (80-.). **265**, 5 (1994).
[43] S. Plimpton, J. Comp. Phys. **117**, 1 (1995).
[44] S. Gruber, C. H. Haering, and K. Nasmyth, Cell **112**, 765 (2003).
[45] J. K. Ryu, A. J. Katan, E. O. van der Sluis, T. Wisse, R. de Groot, C. Haering, and C. Dekker, bioRxiv , 2019.12.13.867358 (2019).
[46] K. Kimura and T. Hirano, Cell **90**, 625 (1997).
[47] K. Kimura, V. V. Rybenkov, N. J. Crisona, T. Hirano, and N. R. Cozzarelli, Cell **98**, 239 (1999).
[48] E. Kim, A. M. Gonzalez, B. Pradhan, J. Van Der Torre, and C. Dekker, bioRxiv , 2021.05.15.444164 (2021).
[49] S. K. Nomidis, M. Caraglio, M. Laleman, K. Phillips, E. Skoruppa, and E. Carlon, Phys. Rev. E , 022402 (2019).
[50] M. Srinivasan, J. C. Scheinost, N. J. Petela, T. G. Gligoris, M. Wissler, S. Ogushi, J. E. Collier, M. Voulgaris, A. Kurze, K. L. Chan, B. Hu, V. Costanzo, and K. A. Nasmyth, Cell **173**, 1508 (2018).
[51] Y. Kim, Science **366**, 1345 (2019).